Effect of Internal Architecture on the Assembly of Soft Particles at Fluid Interfaces

Supporting Information

Jacopo Vialetto,[*,†] Fabrizio Camerin,[*,‡,¶] Fabio Grillo,[†] Shivaprakash N. Ramakrishna,[†] Lorenzo Rovigatti,[§,‡] Emanuela Zaccarelli,[*,‡,§] and Lucio Isa[*,†]

†*Laboratory for Soft Materials and Interfaces, Department of Materials, ETH Zürich, Vladimir-Prelog-Weg 5, 8093 Zürich, Switzerland*

‡*CNR Institute for Complex Systems, Uos Sapienza, P.le A. Moro 2, 00185 Roma, Italy*

¶*Department of Basic and Applied Sciences for Engineering, Sapienza University of Rome, via A. Scarpa 14, 00161 Roma, Italy*

§*Department of Physics, Sapienza University of Rome, P.le A. Moro 2, 00185 Roma, Italy*

E-mail: jacopo.vialetto@mat.ethz.ch; fabrizio.camerin@gmail.com; emanuela.zaccarelli@cnr.it; lucio.isa@mat.ethz.ch

Supplementary Experimental Data

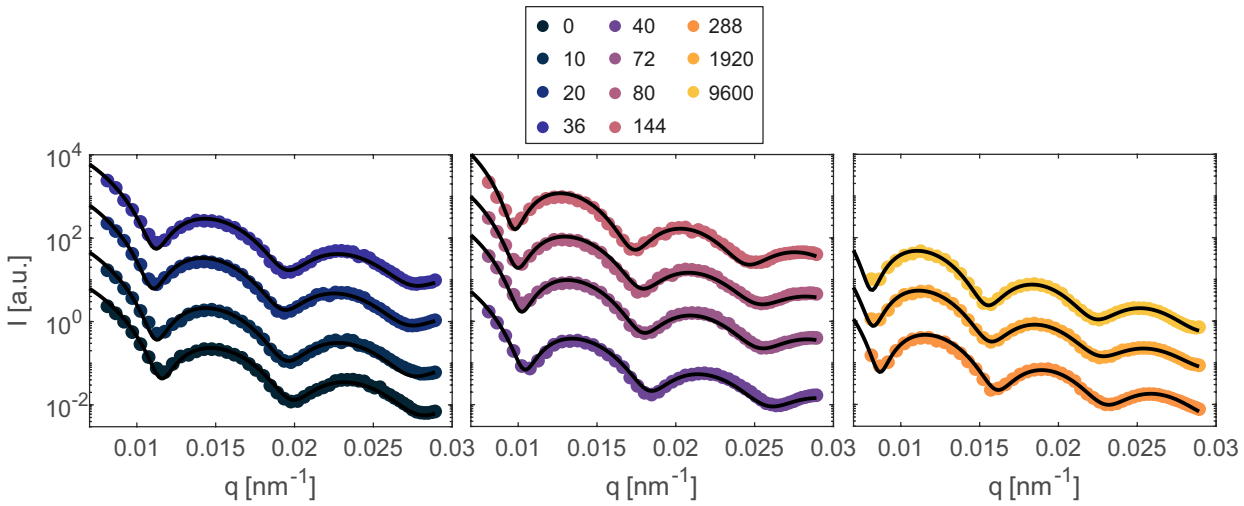

Figure S1: **Form factors of core-shell microgels as function of core removal.** Experimental form factors obtained from SLS experiments at 25°C as function of the core degradation parameters $n \cdot t$ reported above the graphs, arbitrarily rescaled on the y-axis for clarity. Black lines are fits (see Methods).

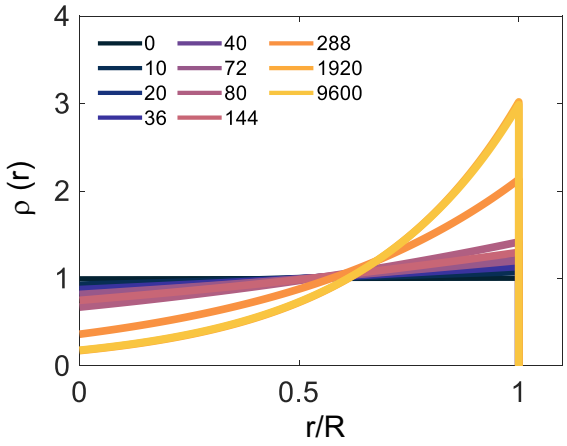

Figure S2: **Density profiles of core-shell microgels as function of core removal.** Microgel radial density profiles ($\rho(r)$) plotted as a function of a normalized radial coordinate r/R, where R is the particle radius, as extracted from the fitting procedure of the experimental form factors, as explained in the Methods section.

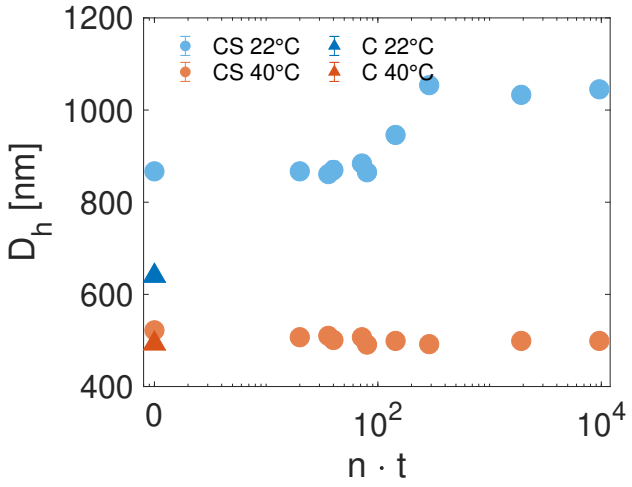

Figure S3: **Microgels' characterization by DLS.** Experimental hydrodynamic diameter D_h for the core (triangles) and core-shell microgels as a function of the core degradation process (circles), expressed as $n \cdot t$, at 22°C and 40°C. Error bars indicate the standard deviation of 4 measurements consisting of 13 runs each and are smaller than the symbols size.

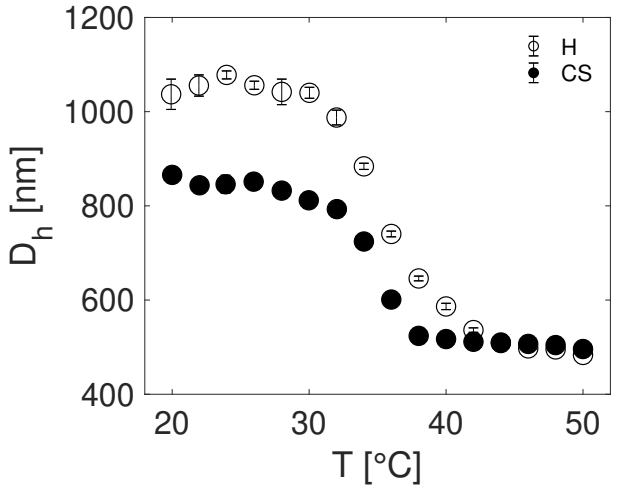

Figure S4: **Hydrodynamic diameter *vs* temperature.** Hydrodynamic diameter D_h for core-shell (filled symbols, corresponding to $X = 0\%$) and hollow (hollow symbols, $X \simeq 100\%$) as function of the solution temperature. Error bars indicate the standard deviation of 4 measurements consisting of 13 runs each and are smaller than the symbols size.

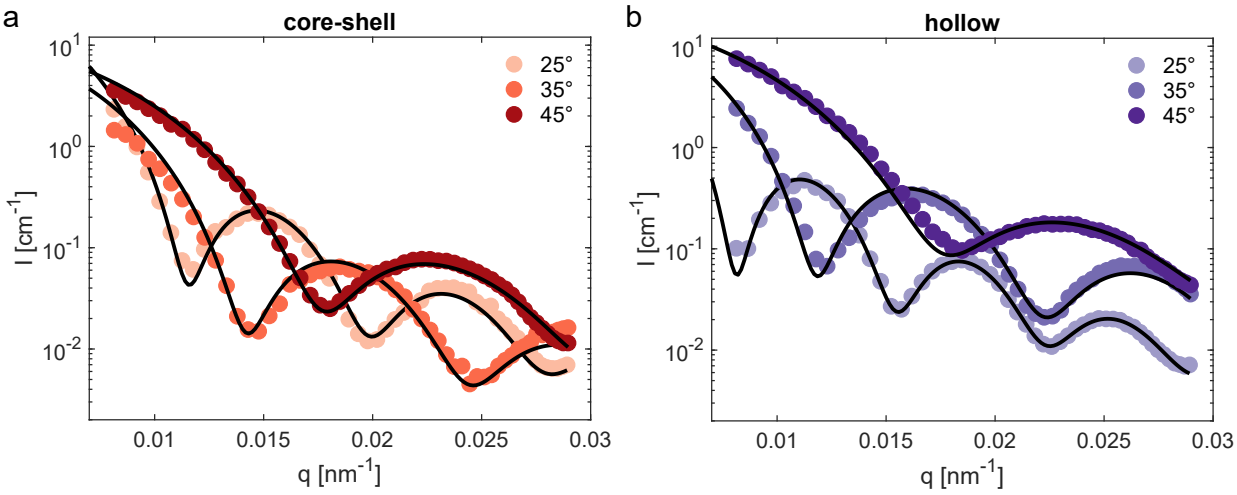

Figure S5: **Form factors of core-shell and hollow microgels *vs* temperature.** a) Form factors (circles) and fits (solid lines) of the core-shell microgels ($X = 0\%$) in aqueous solution at different temperatures. b) Form factors (circles) and fits (solid lines) of the hollow microgels ($X \simeq 100\%$) in aqueous solution at different temperatures.

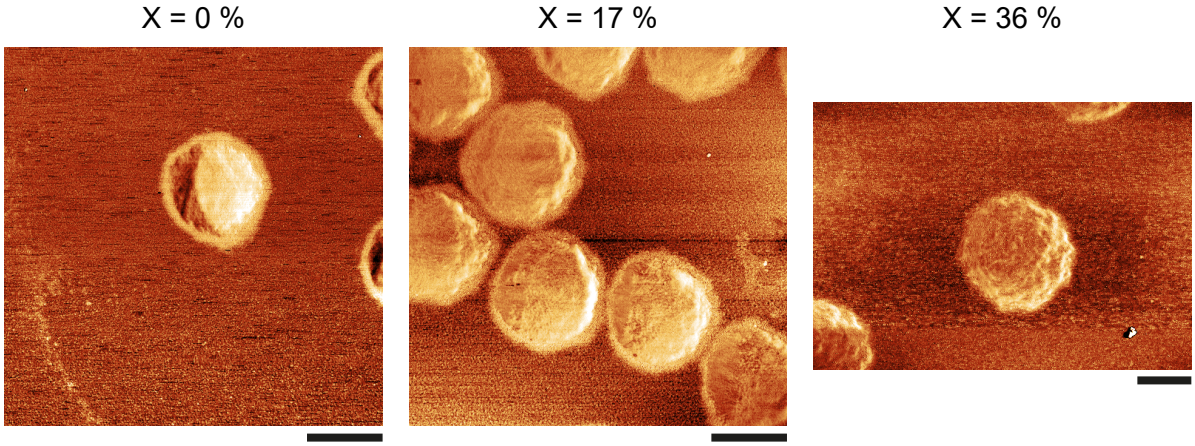

Figure S6: **AFM phase images of individual microgels as function of core removal (X).** Microgels are first adsorbed at the hexane-water interface, and then transferred onto a silicon wafer for imaging. The phase contrast reveals the presence of an extended outer corona surrounding the microgels, which is not evident in height images due to the very low thickness of the polymer layer. AFM phase images of the hollow microgel are in Fig. 5(a). Scale bar: 1 μm.

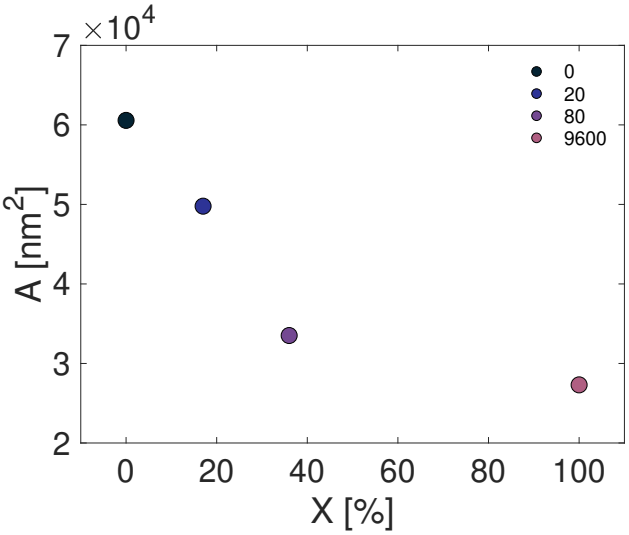

Figure S7: **Total dry mass of microgels as function of core removal.** Area under the AFM height profiles showed in Fig. 3(b) *versus* the degree of core removal X. The integral of the area below the height profiles is a direct measurement of the dry mass of the microgels after deposition. This parameter is equivalent to the volume of the dry particles given the radial symmetry of the height profiles.

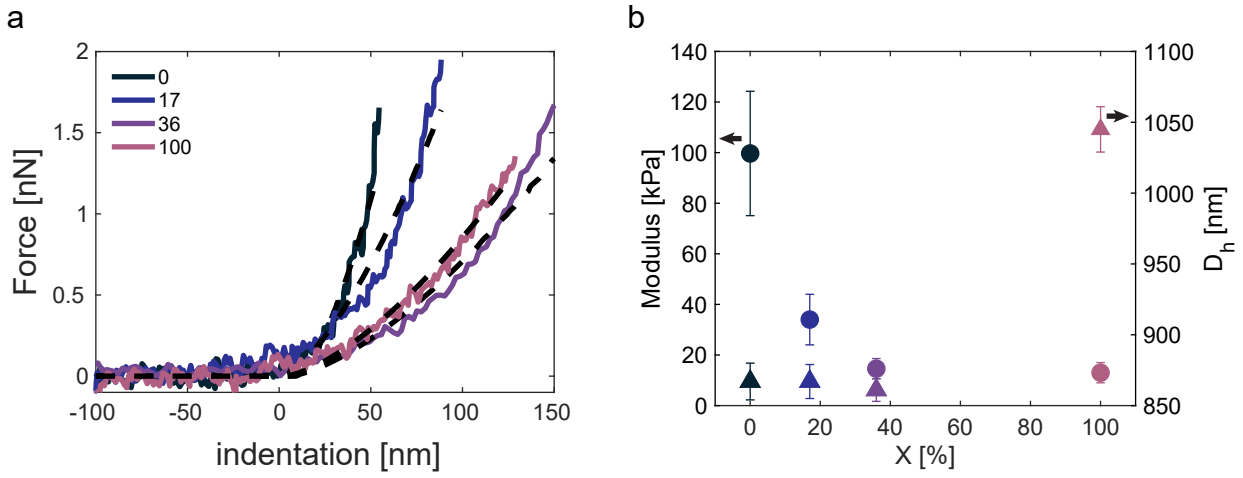

Figure S8: **AFM nano-indentation measurements.** a) Representative AFM force-*vs*-indentation curves obtained at the center of each microgel re-swollen in water after deposition onto a silicon wafer. The colors indicate the different degrees of core removal X. The black dashed lines are the Hertz model fits to the experimental data. b) Average and standard deviation of the microgels Young's modulus (circles, scale on the left axis) and hydrodynamic diameter (triangles, scale on the right axis) as a function of the degree of core removal X.

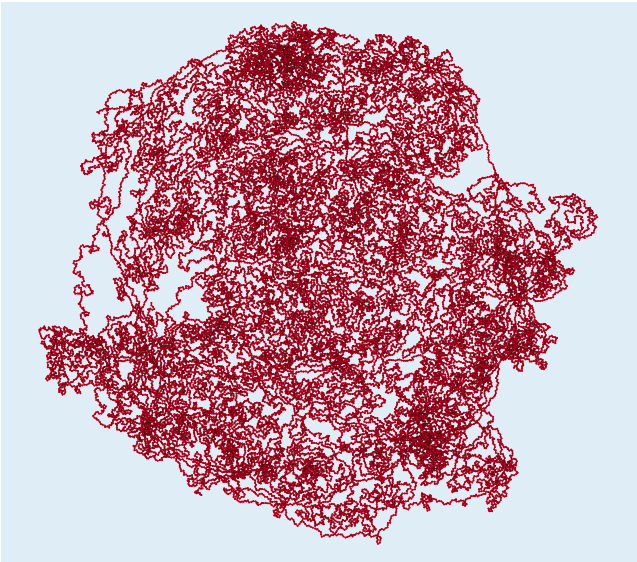

Figure S9: **Simulation snapshot (top view) of a hollow microgel adsorbed at a oil-water interface.**

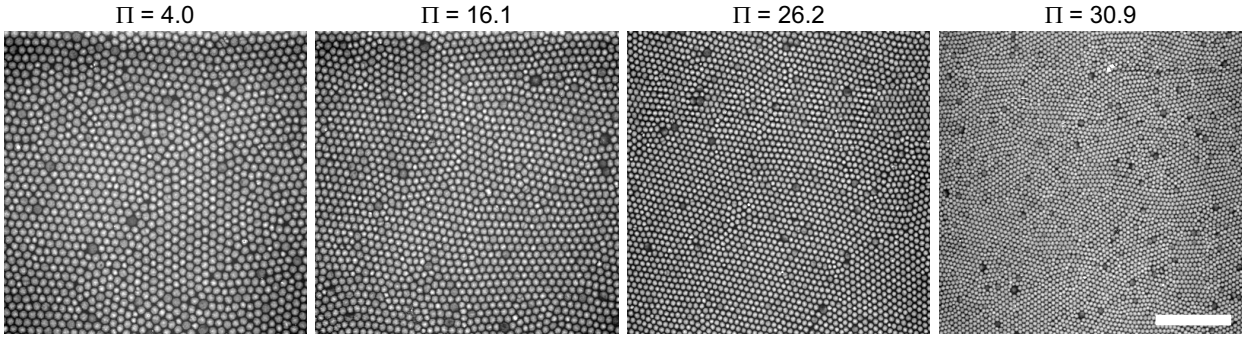

Figure S10: **2D assembly of hollow microgels as function of the surface pressure.** AFM images of the monolayer microstructure after assembly at the hexane-water interface and deposition on the solid substrate, at increasing values of the surface pressure Π. Scale bar: 20μm.

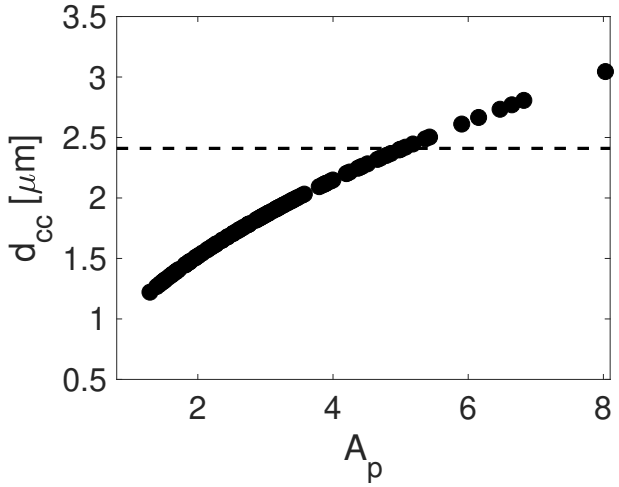

Figure S11: **Average center-to-center distance *vs* area per particle.** Plot of the center-to-center distance d_{cc} as function of the area per particle A_p from images as the ones in S10. The surface pressure of the interface increases from left to right. The dashed line indicates the average diameter of a hollow microgel at the interface prior to compression D_i^0.

Supplementary Numerical Methods and Data

Comparison between the numerical form factors

In this section, we present some additional analysis we carried out in order to determine the hollow microgel model whose form factor best reproduces the experimental data. As also reported in the main text, the comparison is performed by matching the maximum of the first peak for experimental and numerical form factors and, unless specified, we refer to microgels with $Z = 100\sigma$.

First of all, we consider hollow microgels with varying size of the internal hole with the same average monomer density $\rho = 0.08$ of a standard core-corona microgel, which was found to favorably compare to experimental form factors.[1] As shown in Fig. S12, despite the fact that the first peak describes the experimental data well, the second and the third peak of the numerical form factors are all shifted to higher wavenumbers. By reducing the internal monomer density to $\rho = 0.04$ (Fig. S13), we observe a better agreement, especially for the case with $Z_{in} = 75\sigma$. We thus fix the radius Z_{in} and vary ρ, as shown in Fig. S14.

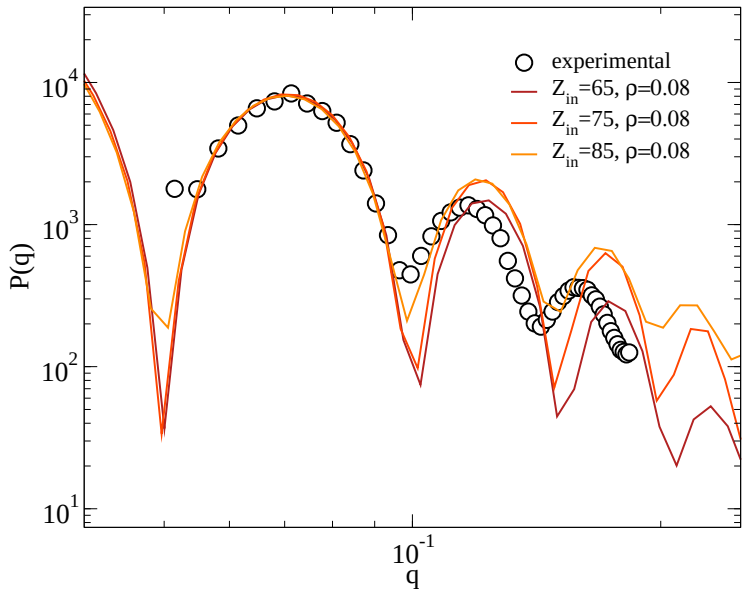

Figure S12: **Form factor comparison for the hollow microgels.** Form factors at a fixed number density $\rho = 0.08$ and outer radius $Z = 100\sigma$, varying the inner size of the cavity Z_{in}. Form factors are arbitrarily rescaled in the x and y-axes and compared to experimental data (symbols).

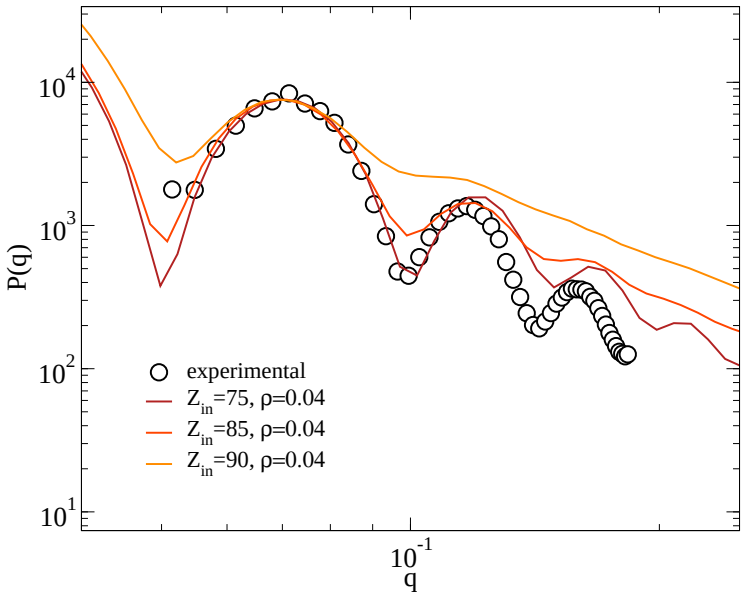

Figure S13: **Form factor comparison for the hollow microgels.** Form factors at a fixed number density $\rho = 0.04$ and outer radius $Z = 100\sigma$, varying the inner size of the cavity Z_{in}. Form factors are arbitrarily rescaled in the x and y-axes and compared to experimental data (symbols).

By reducing ρ, we notice that the position of the peaks in terms of the wavenumber is well reproduced by the $\rho = 0.035$ case.

Finally, we verify the effect of an additional designing force acting on the crosslinkers. This force was previously introduced in the modeling of standard microgels[1] in order to concentrate a higher amount of crosslinkers in the core of the particle, as it is typically seen in precipitation polymerization synthesis protocols. However, as shown in Fig. S15, there is no substantial difference in the form factors for a hollow microgel assembled by employing or not the same designing force used for the standard microgels, and, in particular, the position of the peaks in terms of the wavenumber does not change between the two cases. The minimal differences that remain may be due to small variations in the *in silico* synthesis of the microgels.

Therefore, the hollow microgel model we adopt in the main text is the one with $Z_{in} = 75\sigma$ and an average internal density $\rho = 0.035$, with no additional designing force applied on the crosslinkers during the assembly process. This choice is also found to describe the deswelling transition of the hollow microgels with increasing temperature appropriately, as shown in

Fig.2 of the main text.

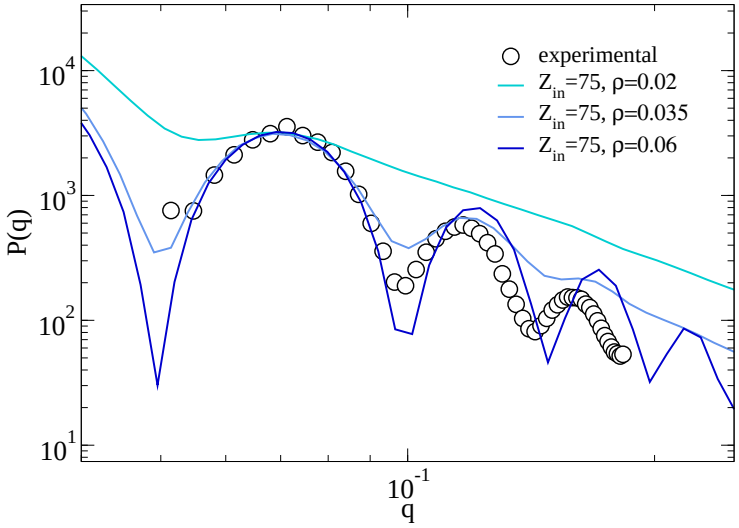

Figure S14: **Form factor comparison for the hollow microgels.** Form factors at a fixed inner radius $Z_{in} = 75\sigma$ and outer radius $Z = 100\sigma$, varying the internal density ρ. Form factors are arbitrarily rescaled in the x and y-axes and compared to experimental data (symbols).

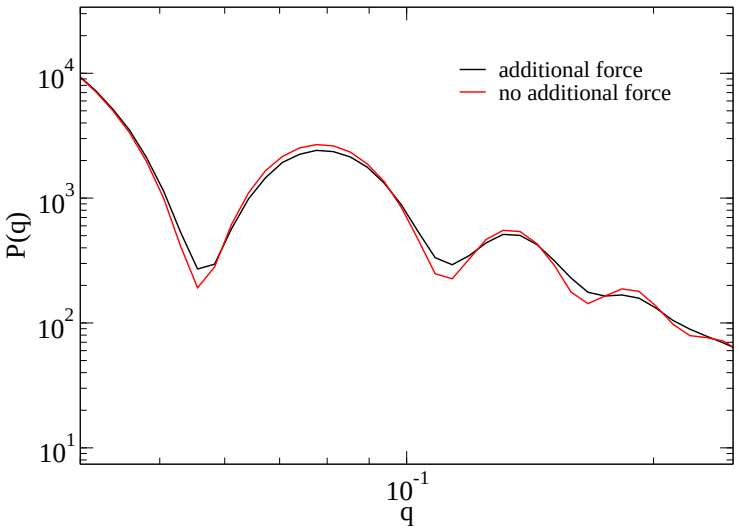

Figure S15: **Effect of the designing force on the form factor of hollow microgels.** The form factors of microgels synthesized with and without a designing force on the crosslinkers are compared. In particular, we consider the case with $Z = 100\sigma$, $Z_{in} = 75\sigma$ and $\rho = 0.035$. Form factors are arbitrarily rescaled in the x and y-axes.

Numerical simulations of the core degradation process

On the numerical side, while it is not possible to faithfully reproduce the chemical stages of the synthesis, we can mimic the core degradation process. In particular, as explained in the main text, we take the hollow microgel whose form factor best reproduces the experimental data and we insert a standard microgel in the central cavity. This corresponds to the experimental state $X = 0\%$, that is the starting core-shell microgel, from which we begin to degrade the core. In simulations, we remove monomers in a random way, progressively reducing the density of the core. Correspondingly, the numerical form factors, as reported in the main text, show a trend in the position of the peaks that closely compares to the experimental one. Additional information comes from the numerical density profiles in real space: while for experiments these are extracted through a fitting procedure, in simulations they can be directly calculated, see Fig. S16. It is evident how, starting from a density profile that resembles that of a standard microgel, the progressive removal of monomers leads to the profile of a hollow microgel. Given the correspondence between numerical and experimental

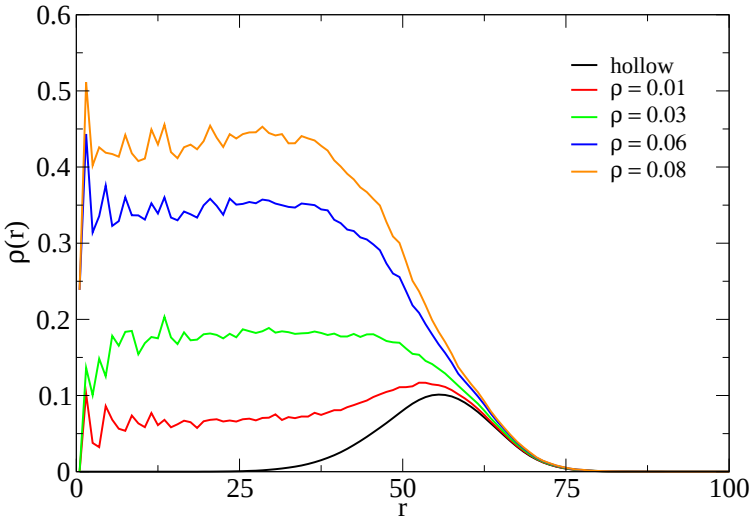

Figure S16: **Effect of the core degradation on the core-shell microgel density profiles.** Radial density profiles of the core-shell microgels obtained by inserting a standard microgel inside a hollow one, and subsequently randomly removing monomers from the core microgel in order to obtain a reduced internal density. The initially inserted standard microgel has a density $\rho = 0.08$, while the hollow microgel density profile corresponds to $\rho = 0$.

form factors, the numerical density profiles constitute a plausible description of the process occurring during the core degradation.

References

1. Ninarello, A.; Crassous, J. J.; Paloli, D.; Camerin, F.; Gnan, N.; Rovigatti, L.; Schurtenberger, P.; Zaccarelli, E. Modeling Microgels with a Controlled Structure across the Volume Phase Transition. *Macromolecules* **2019**, *52*, 7584–7592.